Three-dimensional inverse modeling of the refractive heat-flow anomaly associated with salt diapirism

Seiichi Nagihara

ABSTRACT

This article introduces a technique for three-dimensional inverse modeling of geothermal heat conduction through heterogeneous media. The technique is used to determine the basal geometry of a diapiric salt structure found on the continental slope offshore Texas. Salt is two to four times more thermally conductive than other sedimentary rocks. The geothermal field is perturbed by the presence of salt and results in an anomaly in the heat flow through the seafloor. The spatial variation pattern of the anomalous heat flow reflects the geometry of the salt body. The inverse modeling obtains a model for the thermal-conductivity structure that causes the heat-flow anomaly observed on the seafloor. The inversion algorithm systematically searches for an optimal thermal-conductivity model by iteratively minimizing the misfit between the model-predicted and the observed heat flow. To reduce the problem of nonuniqueness, the inversion incorporates a priori information constrained independently, such as the upper surface geometry of the salt and the lateral extent of the salt body, which can be delineated by a limited coverage of two-dimensional seismic data. In addition, it is assumed that the thermal conductivity of the sedimentary strata surrounding the salt body is well constrained. This inversion method is applied to a heat-flow data set obtained over a salt structure on the Texas continental slope. The salt structure was first surveyed with the single-channel seismic reflection, which yielded the a priori information necessary. The base of the salt was not imaged seismically. Then, three dozen heat-flow measurements were obtained on the seafloor over and off the salt feature. The inverse heat-flow modeling performed here shows that this structure is a salt tongue, which has a diapiric root on one side. According to the most optimal thermal-conductivity model obtained, the root seems to extend to 6 km below the seafloor. Refinement in the model geometry and additional constraints on thermal conductivities of the surrounding

Manuscript received April 25, 2002; provisional acceptance September 25, 2002; revised manuscript received December 27, 2002; final acceptance February 10, 2003.

AUTHOR

SEIICHI NAGIHARA ~ *Department of Geosciences, Texas Tech University, Lubbock, Texas 79409-1053; seiichi.nagihara@ttu.edu*

Seiichi Nagihara is an assistant professor of geosciences at Texas Tech University. He received his B.S. and M.S. degrees (both in geophysics) from Chiba University, Japan. He received his Ph.D. in geological sciences at the University of Texas at Austin. His research interests are in sedimentary basin modeling, geothermal heat and fluid transport, and geospatial information sciences.

ACKNOWLEDGEMENTS

Partial funding for this research was obtained as grants from the Texas Higher Education Coordinating Board and TDI-Brooks International. Comments from John Lorenz, John Doveton, and an anonymous reviewer were helpful in improving the manuscript.

strata should yield a model that is more detailed and would allow more thorough geological interpretation of the salt structure.

INTRODUCTION

The perturbation of the geothermal field associated with salt diaprism has been the interest of many researchers (Selig and Wallick, 1966; Epp et al., 1970; Von Herzen et al., 1972; Lewis and Hyndman, 1976; O'Brien and Lerche, 1984; Nagihara et al., 1992; Corrigan and Sweat, 1995). The thermal conductivity of salt is two to four times greater than that of other sedimentary rocks. A salt diapir, buried in strata of much lower thermal conductivity, funnels geothermal heat flow and causes a high-temperature anomaly in the sediments above. Depending on the geometry of the salt body and its depth of burial, the surface heat flow over the salt can be two to three times greater than that away from the salt.

This phenomenon is important in petroleum exploration and production in two aspects. First, the perturbation of the geothermal field affects the hydrocarbon maturation process in the sediments around the salt diapir (O'Brien and Lerche, 1988; Lerche and Lowrie, 1992; Mello et al., 1995). Second, the surface heat-flow anomaly associated with the salt diapir, if characterized in detail, may provide constraints to the geometry of the salt body (Nagihara et al, 1992). This study focuses on the second. The geothermal field around a salt structure may also be perturbed by fluid and gas migration through the faults associated with salt diapirism, but the fluid-induced heat anomalies are focused around their migration paths (Foucher et al., 1990), and they are of much shorter wavelengths than the conductive anomalies. In addition, fluid-induced thermal anomalies occur only when the flow is active. Researchers can distinguish between the fluid-induced anomalies and those that resulted from spatial variation of thermal conductivity if they obtain a large number of closely spaced heat-flow measurements over the salt structure of interest.

In the northern continental slope of the Gulf of Mexico, large hydrocarbon reservoirs are found beneath sheetlike salt structures that are buried under relatively thin (100–500 m) layers of sediment (Montgomery and Moore, 1997). These salt sheets originate from massive evaporites deposited during the Jurassic (Salvador, 1987, 1991). Overburden of younger sediments has squeezed a large part of the salt to shallower depths. Individual allochthonous salt features on the continental slope can have very different emplacement histories and structures. Some salt sheets form giant wedges extending from the depocenter near the Gulf Coast to the continental slope (Worrall and Snelson, 1989). In some cases, such wedges are partitioned into smaller pieces because of local sedimentary-loading effects (Seni and Jackson, 1992). Linear salt wedges and salt walls, once squeezed into shallow strata, tend to flow downslope and form salt tongues. Neighboring salt tongues sometimes coalesce and form large, continuous structures called ''salt canopies'' (Jackson and Talbot, 1989; Jackson and Talbot, 1991). A salt canopy may retain more than one feeder beneath it. The bottom geometry of such salt features is commonly more complex than their surface geometry.

Knowledge of the basal geometry of the salt structure is the key information in the subsalt exploration efforts in the Gulf of Mexico. State-of-the-art, three-dimensional (3-D) seismic techniques can image bases of salt sheets, but have some difficulty in constraining the diapiric roots or feeders hidden beneath the salt sheets (Ratcliff et al., 1992; Ratcliff and Weber, 1997). In such circumstances, detailed observation of the salt-induced heat-flow anomaly may provide the researchers with additional information on its geometry.

Some previous researchers have attempted to constrain the salt geometry in terms of the thermal-conductivity structure by performing trial-and-error, interactive forward thermal modeling (Jensen, 1983; Vizgirda et al., 1985; O'Brien and Lerche, 1988). However, because the computation is rather time consuming, only a limited number of models can be tested in this manner, although there are many loosely constrained parameters. There is no guarantee that the accepted model is the best one among all possible models. In addition, most of these earlier studies performed thermal modeling in two dimensions and did not fully account for the salt-induced refractive heat flux in three dimensions. A 3-D inversion method, if it can be developed, is more advantageous in that it yields statistical measures for the quality and the uncertainty of the model generated.

The inverse modeling may still suffer from the problem of nonuniqueness. In other words, there can be many different thermal-conductivity models that yield similar fits to the observed data. Thus, the researchers must utilize any prior information available on the salt structure to reduce the uncertainty. In case of the subsalt exploration in the Gulf of Mexico, it is most likely that the salt structure of interest already has

a reasonably good coverage of two-dimensional (2-D), seismic grid survey data. Although such data are not adequate for subsalt imaging, they can delineate the lateral extent and the upper surface geometry of the salt in reasonable detail (Watkins et al., 1996). Thus, as a practical matter, the salt top geometry is known a priori. In addition, the researchers know typical thermal-conductivity values for the salt and other sedimentary rocks based on previous measurements made on samples obtained elsewhere (Yang, 1981; Brigaud et al., 1990; McKenna et al., 1996). Utilization of such information reduces the nonuniqueness problem.

The present work introduces a technique for 3-D inverse modeling of refractive heat conduction, using the salt-induced anomaly as an example. The specific objective here is to constrain the geometry of the salt body, given the surface heat-flow data that characterize the conductive anomaly in detail (Figure 1). This technique takes advantage of the types of a priori information mentioned above and dramatically reduces the problem of nonuniqueness.

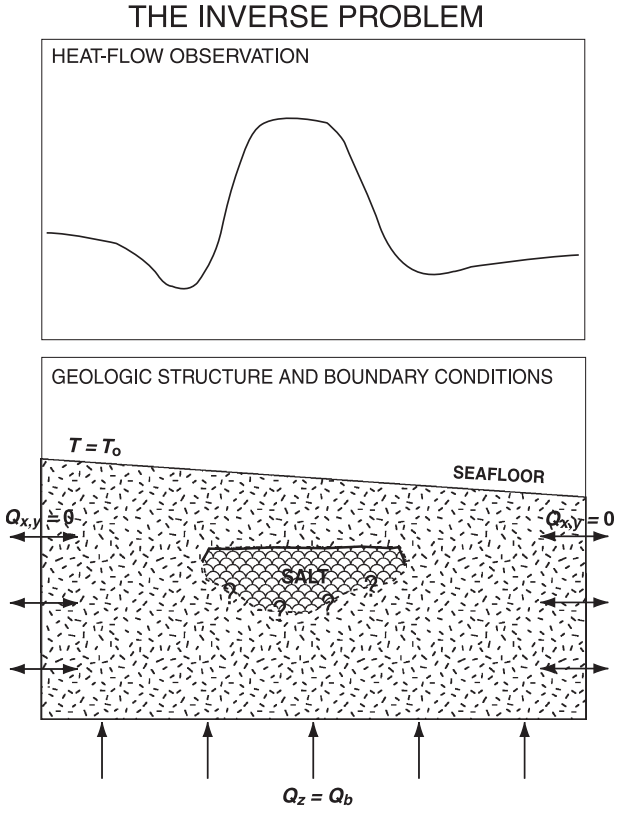

Figure 1. Conceptual diagram describing the problem of inverting the observed heat-flow anomaly for the geometry of a salt. The boundary conditions for the thermal modeling are also described.

MODELING METHODOLOGY

Inversion Based on the Simulated-Annealing Algorithm

The inverse problem defined here is to obtain an optimal model of thermal-conductivity distribution ($\boldsymbol{K}$) for a given set of surface heat-flow observations (Figure 1), whereas the forward problem is to obtain the heat-flow field for a given thermal-conductivity structure. The present work deals with a relatively simple case in which the seafloor is flat and isothermal at a temperature designated T_0. The bottom of the model volume has a fixed input of vertical heat flow (Q_b). No lateral heat exchange occurs at the sides of the model volume. The salt body here is much smaller than the dimensions of the entire model volume, and so the boundary conditions have little influence on the thermal anomaly associated with the salt.

As explained in the Appendix, the forward problem given here can be solved only numerically. The present work uses the finite difference method (Weinstein et al., 1969; Smith, 1985) by dividing the model volume into small rectangular blocks. In solving the inverse problem, the traditional least-squares approach (e.g., Meju, 1994), which requires the forward problem to be solved analytically, is not useful in this case. The inversion method presented here is based on the simulated-annealing algorithm (Kirkpatrick et al., 1983; Sen and Stoffa, 1995), which can be used in nonlinear problems. In performing the inverse modeling based on simulated annealing, one first defines the objective function, which needs to be minimized. Here, the square-sum of the differences between the measured and model-predicted heat-flow value at each observation point is the objective function:

$$E(\boldsymbol{K}^m) = \sum_{l=1}^{L} \left(q_l^{\mathrm{o}} - q_l^{\mathrm{m}}\right)^2 \qquad (1)$$

where q_l^{o} and q_l^{m} are the observed and model-predicted heat-flow values at the lth observation location, respectively. $\boldsymbol{K}^m$ is a vector whose elements are the thermal-conductivity values of all the finite difference cells.

The simulated-annealing algorithm searches through the model parameter space using a sampling technique similar to the Monte Carlo method. In the Monte Carlo method, samples are drawn in a purely random fashion. In other words, each possible set of parameters (statistical event) has the same probability of being picked. In simulated annealing, samples are drawn from a biased (nonuniform) probability distribution (Kirkpatrick et al., 1983; Sen and Stoffa, 1996). Thus, certain parameter

combinations are accepted with higher probabilities than others. There are several different ways of implementing simulated annealing into a computation algorithm. The present work uses the Metropolis simulated-annealing algorithm (Metropolis et al., 1953).

The algorithm starts with a model (i.e., one set of parameters) $\boldsymbol{K}^m$ chosen at random. Then, it obtains the temperature distribution for the model by solving the forward problem (see Appendix) and yields the surface heat-flow value at each surface grid cell location:

$$q_{i,j}^{\mathrm{m}} = \frac{T_{i,j,2} - T_{i,j,1}}{\Delta z} K_{i,j,1/2} \tag{2}$$

where $T_{i,j,k}$ and $K_{i,j,k}$ are the temperature and the thermal conductivity at coordinate (i,j,k), respectively, and Δz is the thickness of the surface grid cell. The model-predicted heat-flow value at the lth observation point (q_l^{m}) is represented by the heat-flow value obtained for the grid cell in which the lth point is located.

Once q_l^{m}s are determined, the error of this model, $E(\boldsymbol{K}^m)$ can be obtained from equation 1. Next, a new model, $\boldsymbol{K}^{m+1}$ is generated by slightly perturbing $\boldsymbol{K}^m$. $E(\boldsymbol{K}^{m+1})$ is then computed. If

$$\Delta E = E(\boldsymbol{K}^{m+1}) - E(\boldsymbol{K}^m) \tag{3}$$

is zero or negative, the new model is accepted, because this means that the overall fit between the model-predicted heat flow and the observed heat flow has improved by the model perturbation. If ΔE is positive, the new model is accepted with a probability:

$$P = \exp\left(-\frac{\Delta E}{\Theta}\right) \tag{4}$$

where Θ is a control parameter, which is commonly called ''temperature'' (Sen and Stoffa, 1995). The present study, however, does not follow this terminology to avoid the confusion with the real temperature (T). Thus, Θ is simply called the simulated-annealing iteration control parameter here. The model acceptance rule described above is known as the Metropolis criterion. The model perturbation and acceptance routine is repeated until $E(\boldsymbol{K}^m)$ no longer decreases after many iterations while Θ is gradually reduced toward zero.

The simulated-annealing algorithm is effective if $E(\boldsymbol{K}^m)$ has more than one minimum. If the algorithm accepts a new model only if ΔE is negative without the Metropolis criterion, it finds a minimum closest to the starting model, and then the search will stop. However, this minimum may not necessarily be the global minimum. With the Metropolis criterion, even a new model that does not improve the fit can still be accepted with a certain probability. This allows the model search to jump out of local minimums. This acceptance probability (P) is greater in the beginning of the iterative model search because of the relatively large Θ value. As Θ approaches zero after several iterations, P becomes smaller. Then, the algorithm starts rejecting models that do not improve the fit.

The manner in which Θ approaches zero is normally prescribed as a function of the number of iterations. This is called the ''cooling schedule.'' If the cooling schedule is

$$\Theta(m) = \frac{\Theta_0}{\ln(m)} \tag{5}$$

where $\Theta(m)$ is the simulated-annealing control parameter at iteration m and Θ_0 is the initial control parameter, convergence to the global minimum can be guaranteed (Sen and Stoffa, 1995). However, iterations based on this cooling schedule converge very slowly. As an alternative,

$$\Theta(m) = \Theta_0 D^m \tag{6}$$

where D is a constant decay factor, is commonly used instead (Chunduru et al., 1995; Sen and Stoffa, 1995). Choices of proper Θ_0 and D are problem dependent. At each cooling step, several model perturbations are performed, and the Metropolis criterion is applied at each perturbation. The total number of required perturbations depends on the total number of the model parameters, but there are no exact formulas that dictate the relationship between the two.

Adaptation of Metropolis Simulated Annealing to the Subsalt Problem

In adapting the Metropolis simulated-annealing algorithm to the subsalt problem, the present work makes the following four sets of assumptions. First, the lateral extent of the salt structure of interest is known a priori. Second, the geometry of the upper surface of the salt body has been constrained a priori. Third, the salt forms a single, continuous body. Finally, the thermal conductivities of the rock salt and other types of sedimentary rocks in the area of interest have already been constrained. The approach taken here is similar to the previous work by Nagihara and Hall (2001), who applied Metropolis simulated annealing in inverting gravity anomalies over salt structures.

In the simulated-annealing inversion algorithm described in the previous section, $\boldsymbol{K}^m$ (the thermal-conductivity vector) is the set of model parameters that needs to be perturbed at each iteration step. However, the a priori condition described above allows the perturbation to occur only in certain ways. To implement the perturbation procedure, the present work first defines an alternative model parameter vector, $\boldsymbol{h}$ (Figure 2). Each element of this vector ($\boldsymbol{h}_{ij}$) represents the salt thickness at location (i,j) of the area underlain by salt in the model volume. The computation algorithm perturbs this vector at each simulated-annealing iteration step instead of perturbing $\boldsymbol{K}^m$ directly. $\boldsymbol{h}_{ij}$ has a discrete choice of values that depend on the total number of layers defined in the model volume. Once $\boldsymbol{h}$ is defined, $\boldsymbol{K}^m$ can be determined uniquely in the following manner. First, the depth to the top of the salt at each (i,j) location, $\boldsymbol{s}_{ij}$, is known a priori. Thus, the depth to the bottom of the salt at that location is simply $\boldsymbol{h}_{ij} + \boldsymbol{s}_{ij}$. Knowing the depth range of the salt column at each (i,j) location, the algorithm can assign the thermal-conductivity value for salt $\boldsymbol{K}_{\text{salt}}$ for the grid cells of depth $\boldsymbol{s}_{ij}$ through $\boldsymbol{h}_{ij} + \boldsymbol{s}_{ij}$. The other cells at ($i,j$) are filled with the conductivity values for other, nonsalt strata $\boldsymbol{K}_{\text{sed}}(z)$, which can be a function of depth caused by compaction, lithologic variation, etc. Thermal conductivity of the cells outside the area underlain by salt is simply $\boldsymbol{K}_{\text{sed}}(z)$.

At each model perturbation, the information transfer between $\boldsymbol{h}$ and $\boldsymbol{K}^m$ takes place. All the a priori information (i.e., the lateral extent of the salt, the upper surface geometry, the continuity of the salt body, and knowledge of thermal conductivities for different rock types) is implicitly built into the model perturbation process. This makes the inversion computation efficient. After the algorithm updates $\boldsymbol{K}^m$ at each perturbation, it recalculates the forward heat-flow response of the salt body. Then, it applies the Metropolis criterion.

The entire computational algorithm described above was coded in Fortran 90 for the present work. The model perturbation at each iteration step is performed with

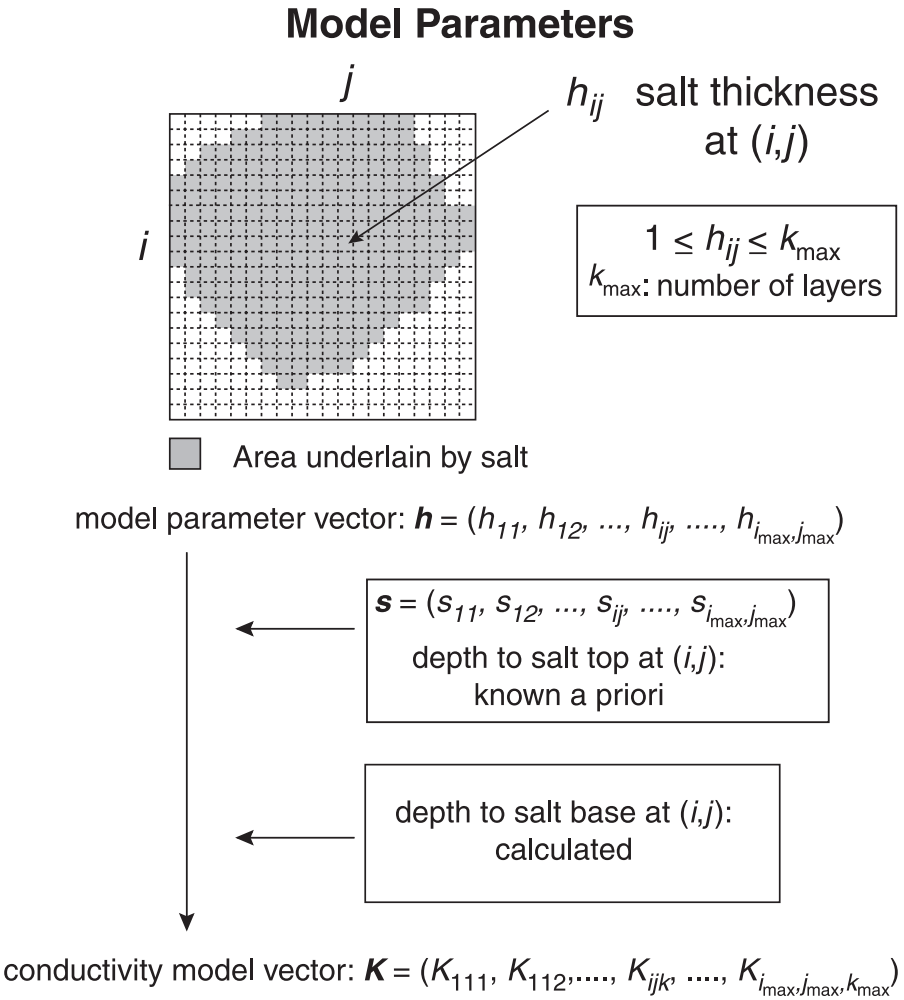

Figure 2. The upper half of the diagram gives a plan view of the source volume, which shows the lateral extent of the area underlain by salt. The lower half of the diagram shows how the information in the model parameter vector $\boldsymbol{h}$, and the prior information (i.e., the depth to the top of the salt and the thermal conductivities of the salt and the nonsalt sediment) are mapped into the conductivity model vector $\boldsymbol{K}$.

the Fortran 90 intrinsic random number generator. The system clock of the computer is used to seed the random number generator, so that a different sequence of numbers occurs every time the code is run (Press et al., 1996).

INVERSION USING REAL HEAT-FLOW DATA

The inversion algorithm, based on simulated annealing, is now applied to a set of heat-flow data previously obtained (Nagihara et al., 1992) over a salt structure located in the middle continental slope offshore Texas (Figure 3a). The structure is buried under a sedimentary cover of 200–500-m thickness. Beckley and Behrens (1993) mapped its lateral extent and upper surface geometry by carrying out a series of single-channel seismic reflection surveys. In a plan view, the salt feature is semicircular with a diameter of approximately 10 km. The seismic data did not image the lower surface of the structure, but based on their examination of the stratigraphy and the faults in the overlying strata, these authors suggested that the structure was a salt tongue rooted at its northwestern edge. The upper surface of the salt shows a linear peak above the suspected root. The seafloor topography also shows a linear peak, but it is slightly offset northwestward from the peak of the salt body (Figure 4). The offset is reasonable if the root is inclined downslope like the roots of other salt tongues found in the vicinity (Liro, 1992; Seni and Jackson, 1992).

Nagihara et al. (1992) obtained about three dozen heat-flow measurements over and off this structure. High (>90 mW/m^2) values, more than twice the values obtained off the salt, were observed over the linear peak of the salt (Figures 3, 4). Based on preliminary 3-D forward thermal modeling, Nagihara et al. (1993) suggested that the large magnitude of the high heat-flow anomaly

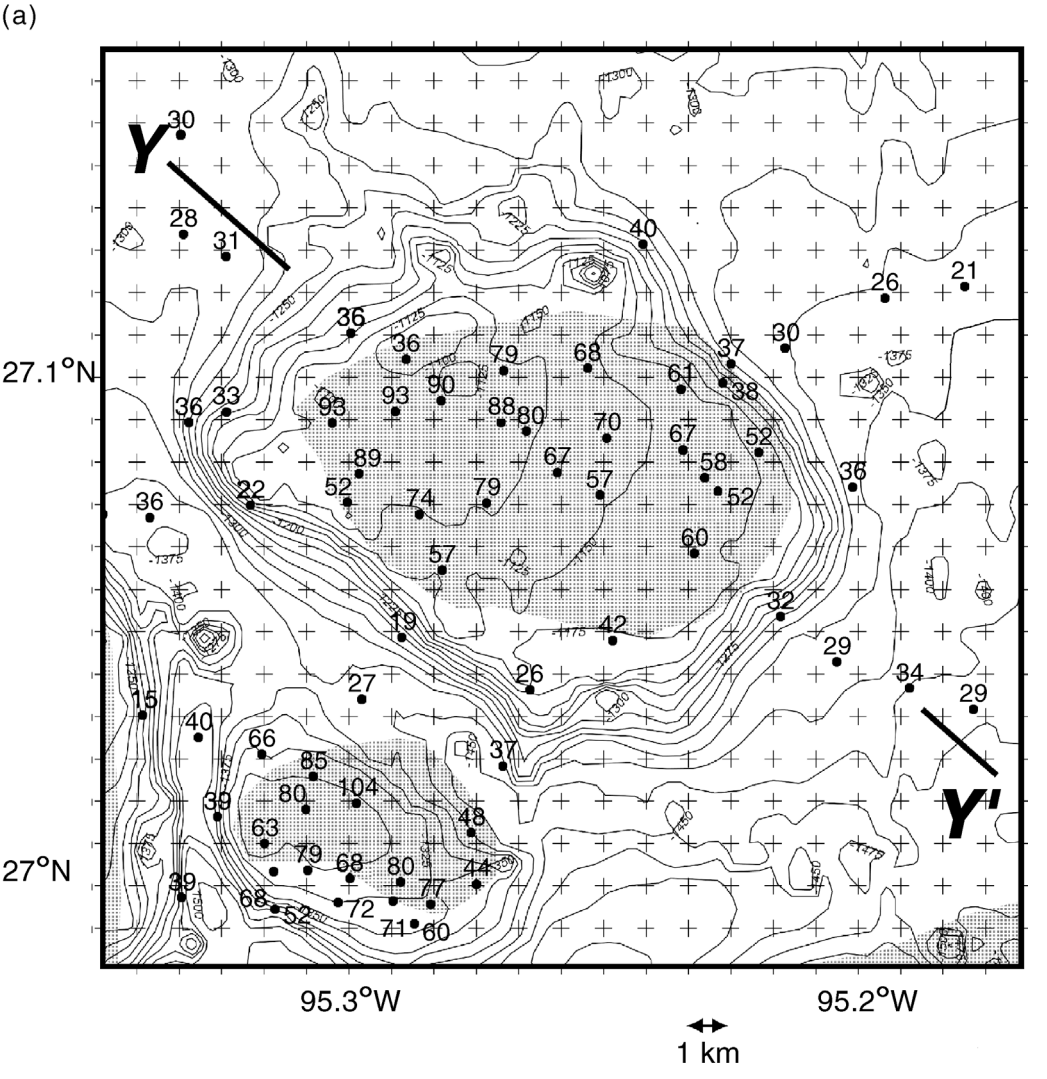

Figure 3. (a) Map showing the extent of the salt structures (shaded) and the heat-flow data (mW/m^2) coverage on the middle continental slope offshore Texas (modified from Nagihara et al., 1992). The greater of the two salt features is modeled in the present study. The grid ticks show the finite difference mesh size (1 km) used in the model. The heat-flow and seismic reflection profiles along YY′ are shown in Figure 4. (b) Upper surface geometry of the model salt shown in a 3-D perspective view.

(b)

Figure 3. Continued.

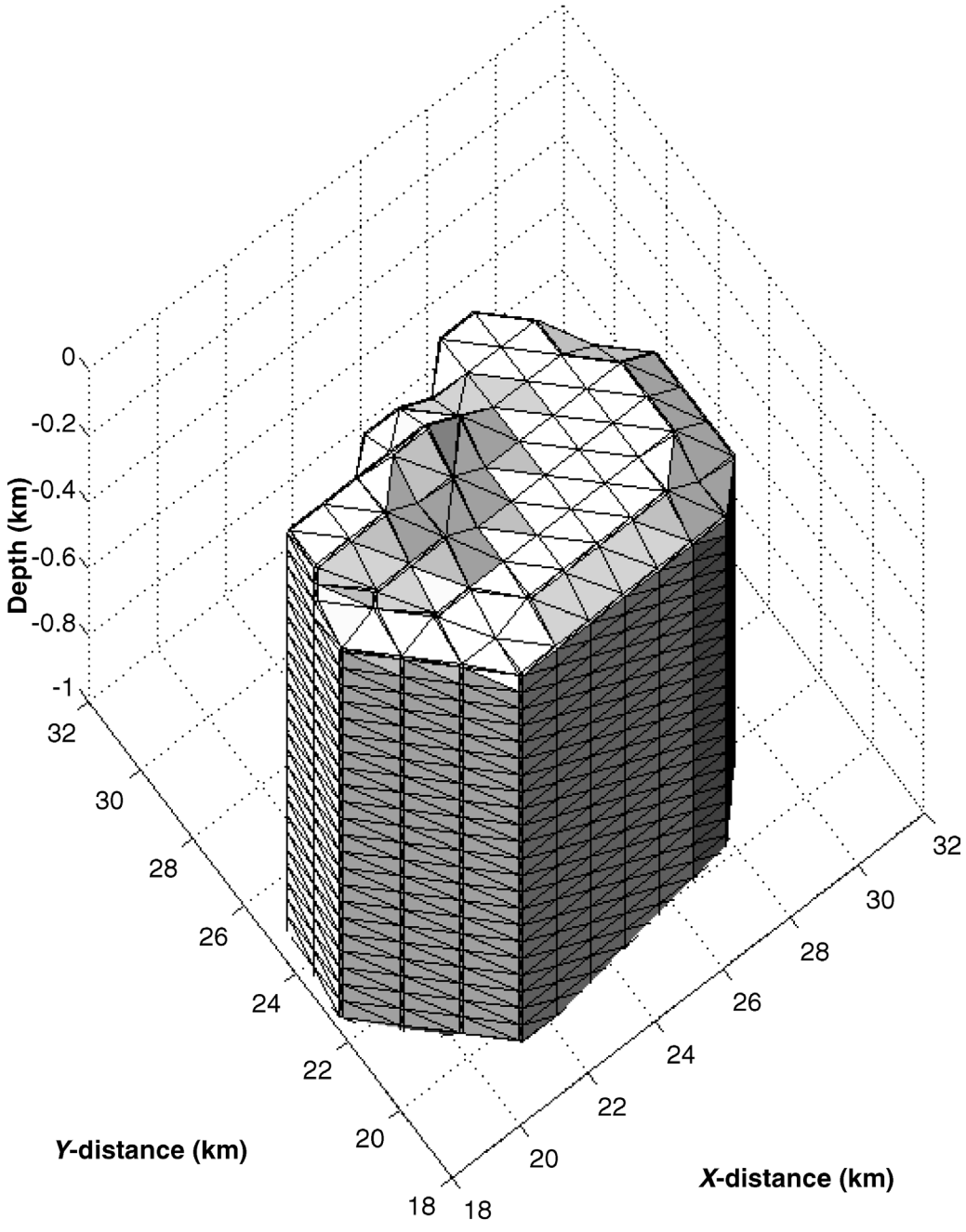

could not be explained if the salt structure had a flat lower surface. In other words, the salt body must be considerably thicker at its northwestern edge than elsewhere. Their finding is consistent with the suggestion made by Beckley and Behrens (1993) that there is a root at the northwestern edge.

In performing the heat-flow inversion, a uniform grid of 1×1 km^2 spacing is applied to the area of interest (Figure 3a). The entire model volume is 50×50 km^2 wide and 15 km deep. Each layer of the volume is 50 m thick. The upper limit of the volume corresponds to the seafloor. The seafloor in the model is flat for simplicity, although in reality there is some topographic variation. The upper surface geometry of the salt body is known a priori (Figure 3b). Thermal conductivity of the salt body is assumed to be uniform at 6 W/mK, although in reality, it varies somewhat with temperature (Yang, 1981). There are no thermal-conductivity data for the sediments surrounding the salt structure, except those at very shallow depths (<5 m below seafloor). It

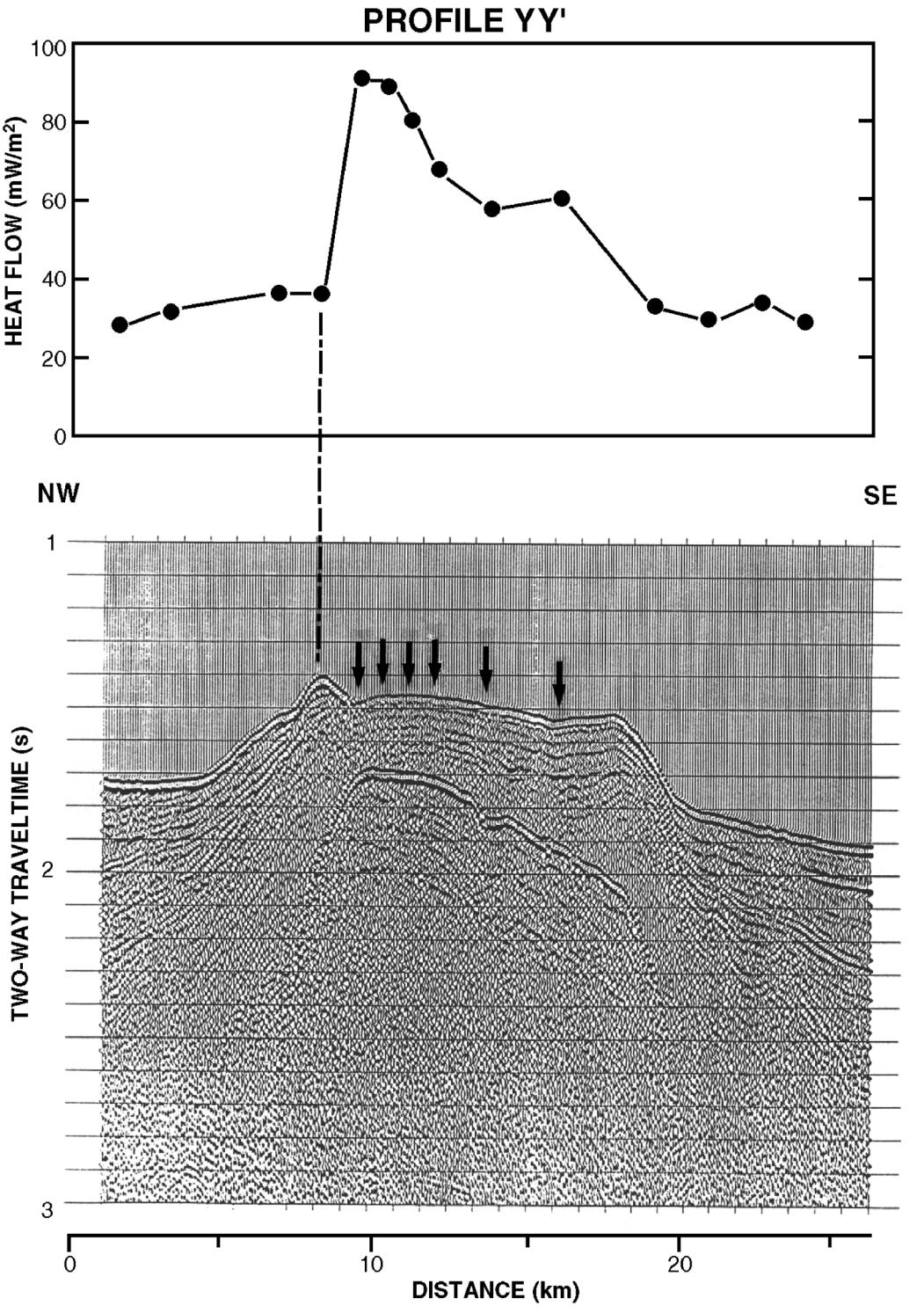

Figure 4. The heat-flow and seismic reflection profiles along YY′ in Figure 3a (modified from Nagihara et al., 1992). As indicated by the dashed line, heat flow is low at the peak of the seafloor topography but greatest over the peak of the salt top.

is assumed that sedimentary thermal conductivity in the model varies stepwise with depth at 1.5 (0–2 km), 2.0 (2–5 km), and 2.5 W/mK (5 km to the bottom). The increase with depth reflects the compaction of the sediments.

Although the model volume extends to 15 km below the seafloor, it is assumed that 8 km is the maximum possible depth the bottom of the salt can reach. The depth limit has been set so that the bottom boundary condition of the model volume does not significantly influence the inversion outcome. One could set a greater depth limit for the bottom of the salt, but the present work does not do so for two reasons. First, a greater depth limit would require a greater model

volume, and thus would require a longer computation time. The inversion code with the current model volume configuration takes almost 2 days to run on a personal computer (Dell PowerEdge 1400). Second, the previous studies in the Texas–Louisiana continental slope suggest that the roots of this type of shallow, allochthonous, tabular salt features are not likely to reach 8 km below the seafloor (Sawyer et al., 1991; Liro, 1992; Seni, 1992). As shown later in this section, the depth limit used here seems adequate, because the base of the salt in the final model does not reach the 8-km depth.

The shallowest limit of $\boldsymbol{h}_{ij}$ perturbation is set at 1.5-km depth below seafloor anywhere in the lateral extent of the salt. It should be reasonable to assume that the bottom of the salt, which does not produce coherent seismic reflection, is at least 1 km thick. The present algorithm perturbs $\boldsymbol{h}_{ij}$ with 500-m increments. There are 14 possible choices for $\boldsymbol{h}_{ij}$ at each (i,j) combination between the 1.5- and 8-km subbottom depths. The area underlain by salt consists of 66 grid cells. Therefore, 14^{66} different combinations of the model parameters are possible. This is still a much smaller number of choices than perturbing $\boldsymbol{K}^m$ directly without any a priori information on the salt geometry. There are 35 locations where heat flow has been measured. The total number of the observation points is roughly half of the number of the model parameters in $\boldsymbol{h}$. Thus, this inverse problem is underdetermined.

The heat flow entering from the bottom of the model volume (i.e., the bottom boundary condition) is uniformly set at 42 mW/m^2. This is the value typically obtained in the western abyssal plain, where data of higher quality were obtained previously (Nagihara et al., 1996). The value is slightly higher than those that actually measured off the salt (Figure 4). However, this is reasonable, because the heat flow through the seafloor off the salt is suppressed by the faster sedimentation there than over the salt. The difference in sedimentation rate occurs because the sediments are being transported downslope and accumulate more in the gaps between the topographic highs associated with salt diapirism. A rough estimation (Nagihara et al., 1993) suggests that the difference in sedimentation causes the heat flow off the salt to be suppressed by 10% relative to that over the salt. The model calculation accounts for the difference.

In applying the simulated-annealing algorithm to the heat-flow data set from the Gulf of Mexico, the present work used a cooling schedule of $\Theta_0 = 1.5$ and $D = 0.95$ for each run. These values were chosen after several trial runs. The salt thickness vector elements were perturbed between the 30th layer and 160th layer with a constant increment of 10 layers. The simulated-annealing iteration stopped at the 200th cooling step. At each step, 20 iterations (model perturbation-acceptance cycles) were performed. The total number of models generated for this inversion was 4000 per run, which is a very small fraction of the entire model parameter space. It is common that researchers perform simulated-annealing computations many times for a given inverse problem. Because the model perturbation sequence is different each time, the resultant thermal-conductivity models from individual runs are not identical, although they are very similar.

Figure 5 shows the final thermal model obtained from one of the simulated-annealing inversion runs for the Gulf of Mexico data. In this diagram, the model volume is sliced at every 0.5 km in depth. In other words, every 10th layer of the model volume is shown starting from the top. The cells with high values (6 W/mK) are salt and those with lower values are nonsalt strata. This inversion result suggests that salt is considerably thicker where the surface heat flow peaks at about 90 mW/m^2 than elsewhere. That is consistent with the previous expectation from the trial-and-error modeling (Nagihara et al., 1993) and the interpretation of the 2-D seismic images (Beckley and Behrens, 1993), which suggested that the featured studied is a salt tongue rooted at the northwest edge. This root appears in all of the inversion results, although they differ slightly in shape.

DISCUSSION AND CONCLUSIONS

One of the major advantages of carrying out an inversion is that it provides an objective measure of the quality of the final model. In the Metropolis simulated-annealing algorithm, one can perform a large number of inversion runs, using a different starting model and a different perturbation sequence each time, and construct a histogram for each model parameter. Previous studies (Sen and Stoffa, 1995, 1996) have shown that those histograms can adequately represent the posterior probability density (PPD) function for estimating the uncertainty of the model parameters.

In the present work, 14 such independent simulated-annealing runs have been performed for uncertainty estimation. A total of 56,000 models have been evaluated in these runs. Generating a PPD-like histogram for all the 66 parameters is rather prohibitive. Thus, the present work has generated the mean thermal-conductivity structure model in Figure 6. In each layer of the model volume, the grid cells with lighter color are accepted as

Figure 5. A layer-slice view of the thermal-conductivity structure model obtained for a single simulated-annealing inversion run. Every 10th layer of the model volume is shown starting from the top. The white (6 W/mK thermal conductivity) grid cells are determined to be salt.

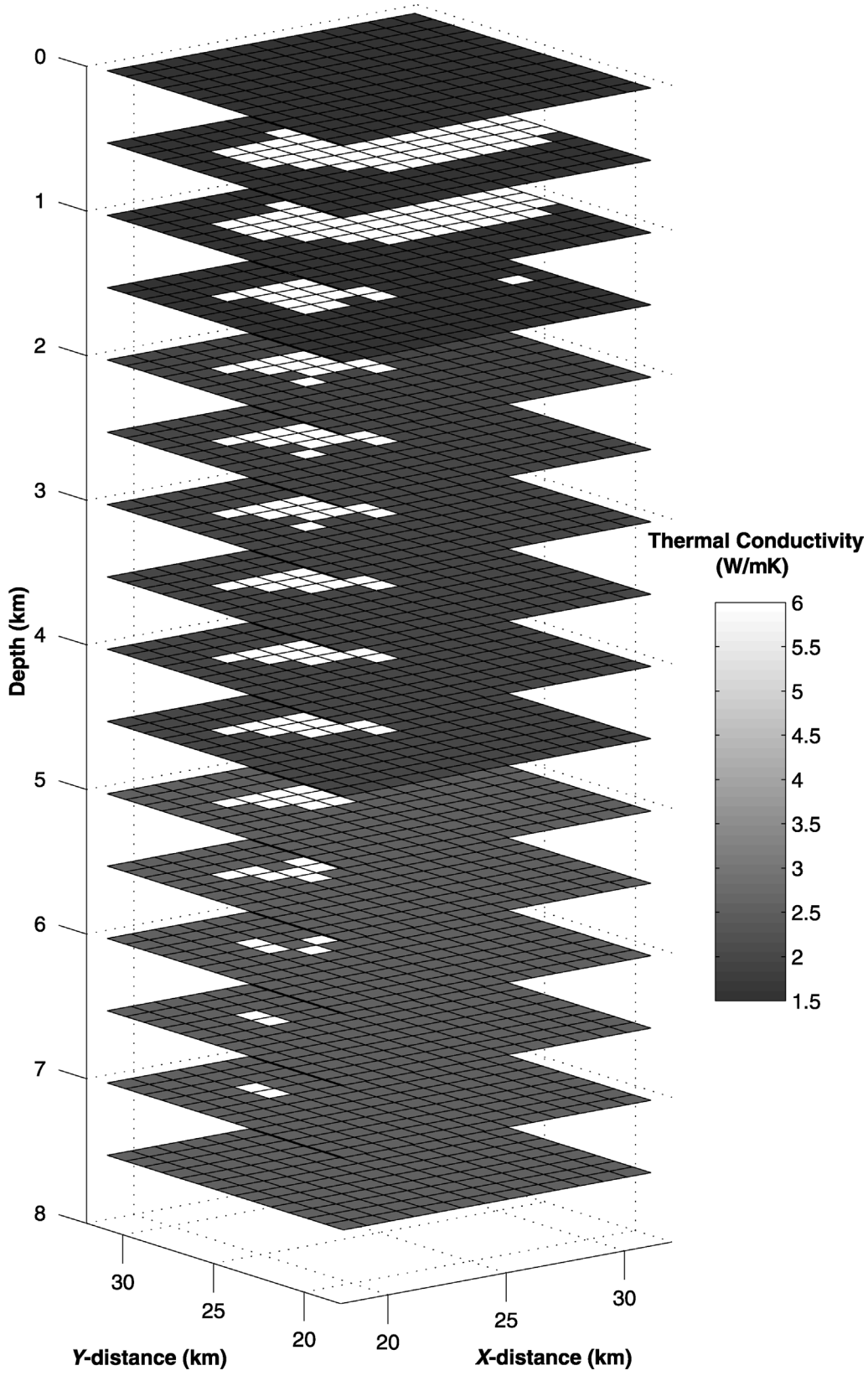

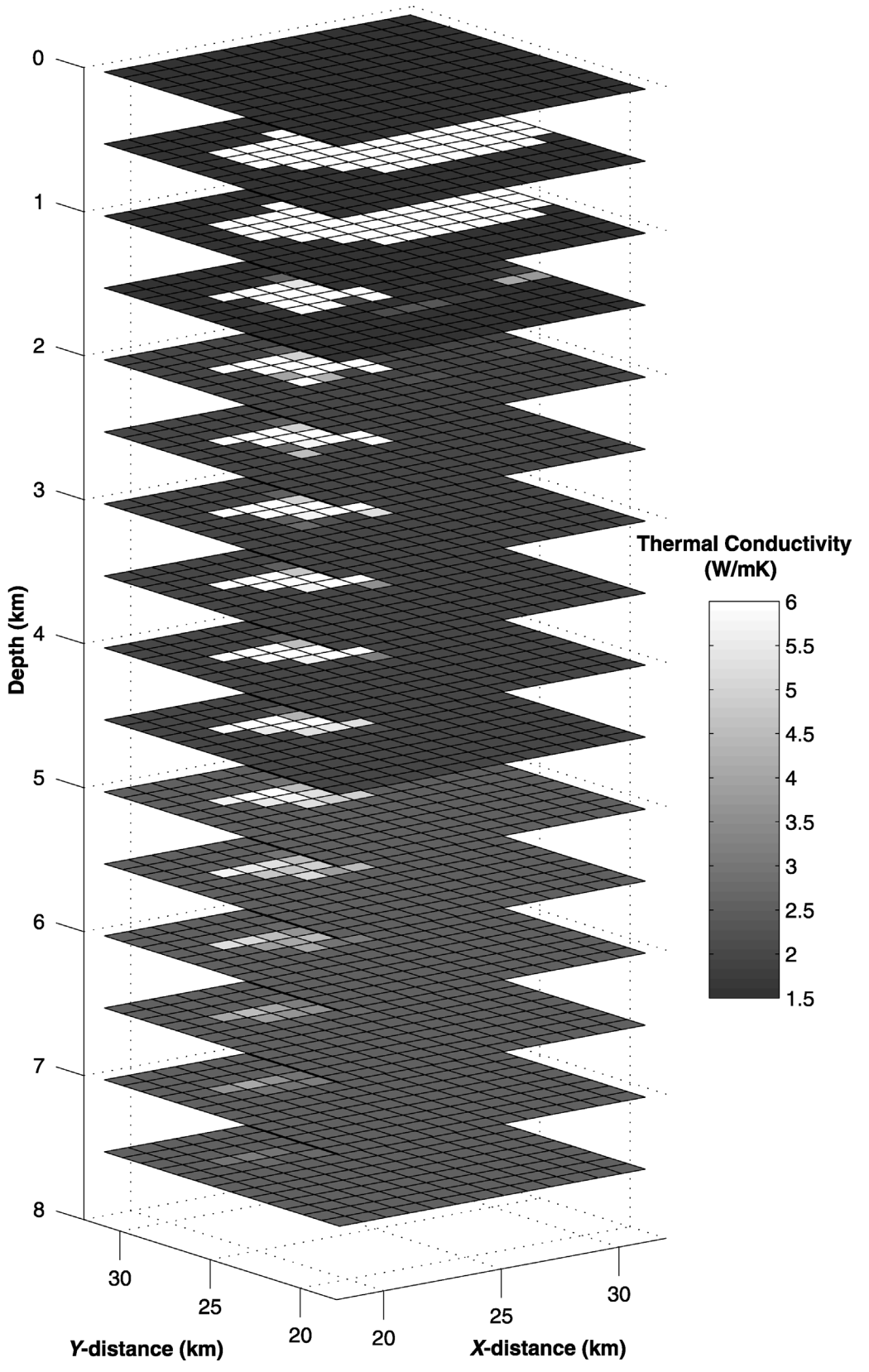

Figure 6. A layer-slice view of the mean thermal-conductivity structure model obtained from 14 independent simulated-annealing runs. Every 10th layer of the model volume is shown starting from the top.

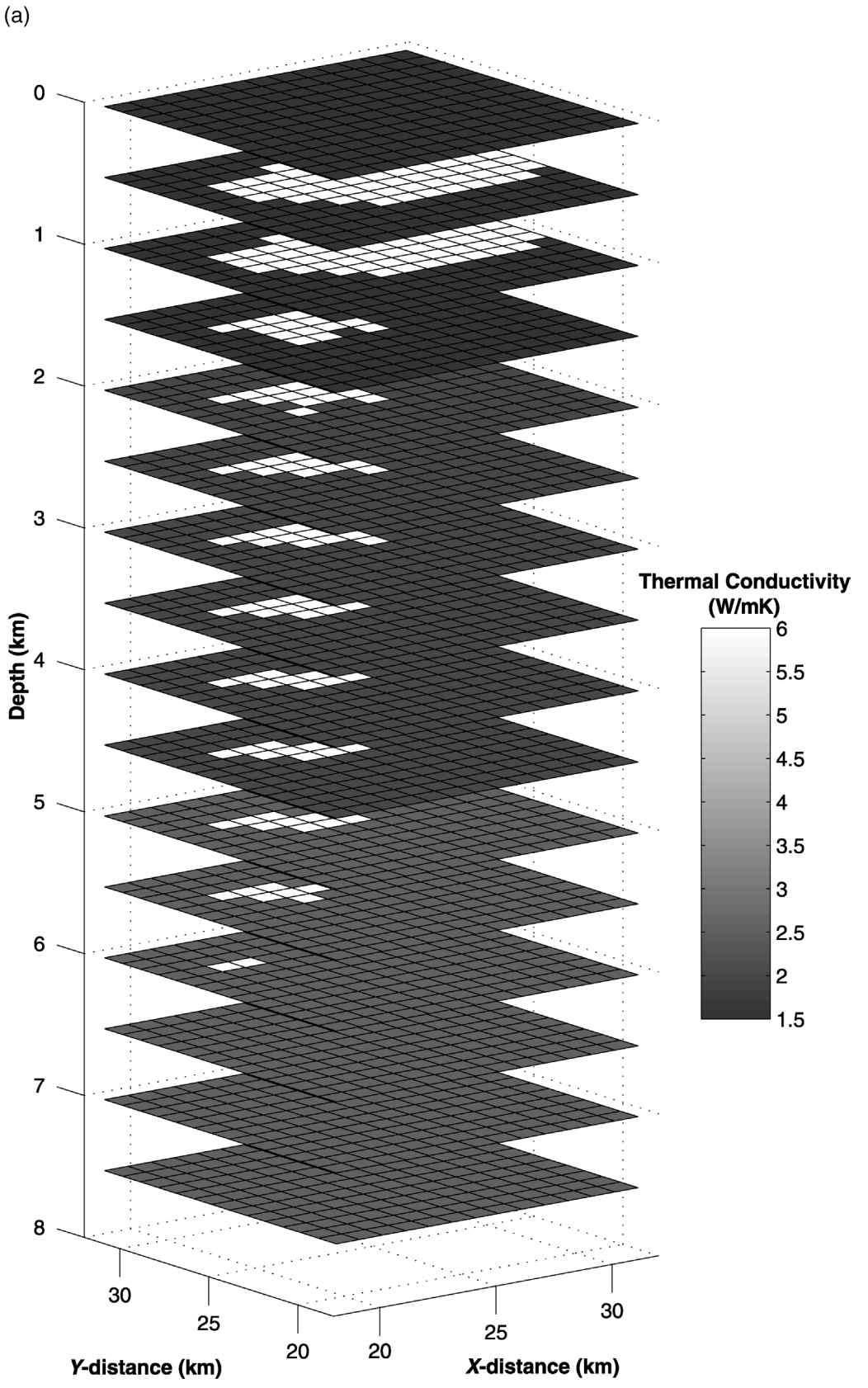

Figure 7. (a) A layer-slice view of the mean thermal-conductivity structure model using only the grid cells that have 60% or greater probability of being salt. Every 10th layer of the model volume is shown starting from the top. (b) A 3-D perspective view of the salt volume for the same mean conductivity model.

(b)

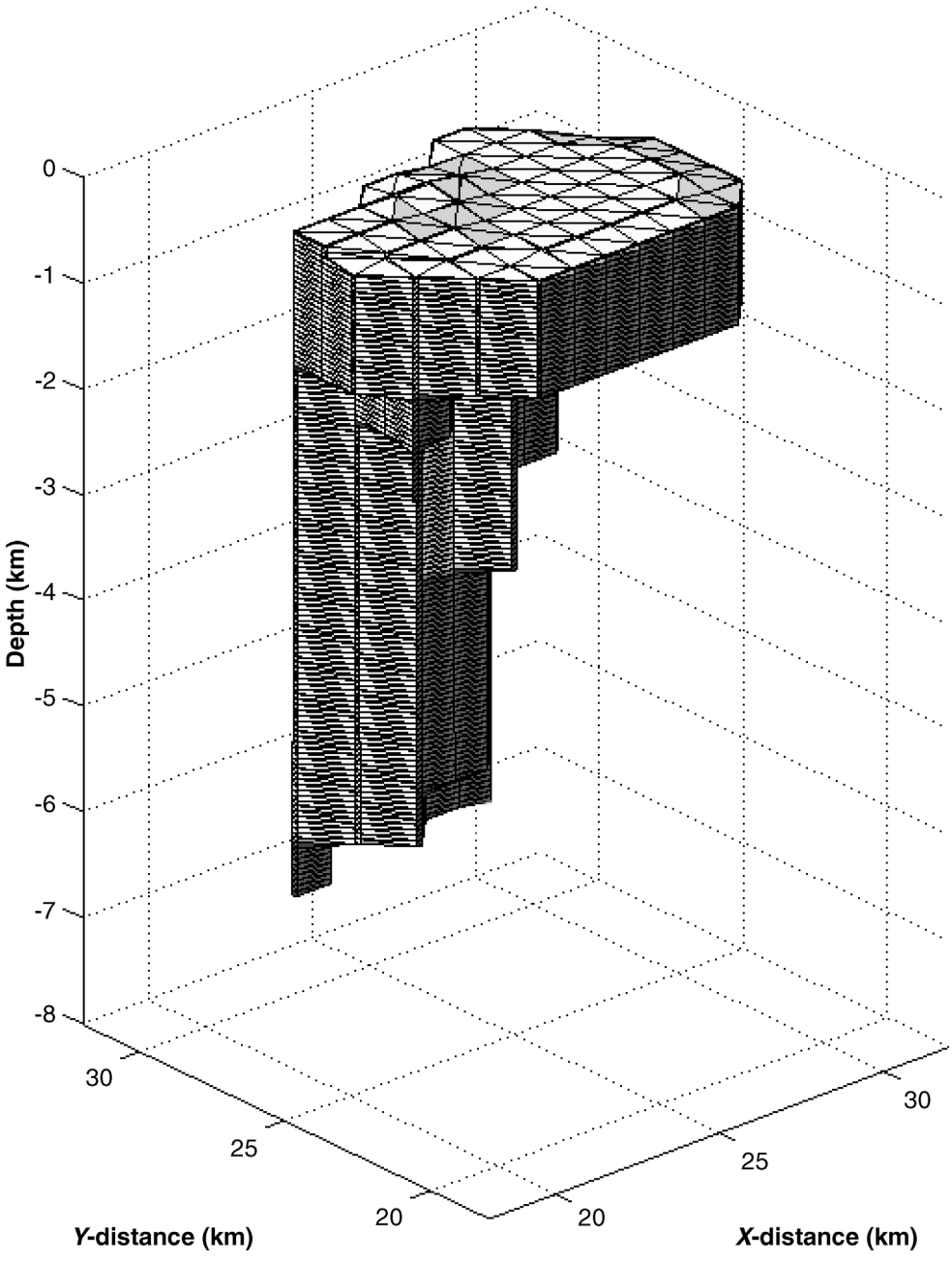

Figure 7. Continued.

salt in the final model more frequently than cells with darker color. The lighter colored cells are therefore more likely to be salt than dark-colored cells. In Figure 7a, cells that are accepted as salt more than 60% of the time are now marked as salt. In this way, the geometry of the salt body can be more clearly defined in a 3-D perspective view (Figure 7b).

It is not the primary objective here to discuss regional geological implications of this inversion result. Obviously, some simplifications have been made in the present model. For example, the thermal conductivity of nonsalt strata in the model is a stepwise function of the burial depth, but in reality, it should vary more gradually in both vertical and horizontal directions. In addition, in the model, thermal conductivity of salt is a constant, but in reality, it varies with temperature (Yang, 1981). Further, the model does not include the thermal effect of the seafloor topography (Blackwell et al., 1980). Potential errors introduced by these simplifications in the model must be thoroughly investigated before any inferences on the salt tectonics and regional geology can be made.

As computers become faster and less expensive with time, one could run the models with much smaller grid spacing and include more geometrical detail. Then, for example, the thermal effect of the seafloor topography could be better accounted for. However, having tighter constraints to the thermal conductivities of the sediments surrounding the salt body would improve the final model most dramatically because it is the contrast in thermal conductivity between the salt and the sediments that produces the heat-flow anomaly. It would be ideal if there have been some deep wells in the vicinity of the salt structure of interest, and they have yielded several core samples from various depths. Then, thermal conductivities can be measured on those cores. If there are no core samples, it would still be helpful to have seismic coverage or well logs that give the porosity or the bulk density of the sediment in the vicinity, from which thermal conductivity can be estimated (e.g., Brigaud et al., 1990).

The major finding of the present work is that by utilizing the simulated-annealing algorithm, it is possible to perform 3-D inverse modeling of steady-state heat conduction through heterogeneous media. In addition, the inversion computation is not very expensive and can be performed on personal computers with reasonable spatial resolution. It has also been shown that the inverse heat-flow modeling can be effective in constraining the basal geometry of laterally extensive, shallow allochthnous salt structures that are rooted at some places, because the refractive heat-flow anomalies over the roots are so large. The problem of nonuniqueness can be reduced if the lateral extent and the upper surface geometry of the salt can be constrained by other means (e.g., seismic profiling). The problem may be reduced further if tight constraints are available for the thermal conductivity of the sediment surrounding the salt structure. In this inversion scheme, all of such prior information is built into the way the model parameter vector is perturbed at each simulated-annealing iteration step. This makes the computation algorithm efficient.

Tabular, allochthnous salt features like the one examined here are commonly found on the continental slope of the Gulf of Mexico and other continental margins (Tari et al., 2002). It is very expensive to survey such salt structures with state-of-the-art 3-D seismic techniques and to process the data. In contrast, acquiring heat-flow data costs much less. This work has shown that inverse heat-flow modeling can be effective in constraining the dipiric roots of shallow salt features. Therefore, there is a good potential that the combination of heat-flow probing and inverse modeling can be developed into a new, economical tool for subsalt exploration.

APPENDIX: SOLUTION OF THE FORWARD PROBLEM

Here, the forward problem is to obtain the heat-flow field for a given thermal-conductivity structure. Mathematically, it is described as a steady-state, boundary value problem, if other environmental factors (e.g., sedimentation, erosion, temporal fluctuation of the surface temperature, pore fluid migration) can be ignored. The governing steady-state heat conduction equation in 3-D (Carslaw and Jaeger, 1959) is expressed as

$$\frac{\partial}{\partial x}\left(K\frac{\partial T}{\partial x}\right)+\frac{\partial}{\partial y}\left(K\frac{\partial T}{\partial y}\right)+\frac{\partial}{\partial z}\left(K\frac{\partial T}{\partial z}\right)=a \tag{7}$$

where T is the temperature, K is the thermal conductivity, and a is the source term.

Figure 1 provides the schematic illustration of the boundary conditions. In the mathematical description of the forward problem, the present work deals with a relatively simple case in which the seafloor is flat and isothermal at T_0. The bottom of the model volume has a fixed input of vertical heat flow (Q_b). No lateral heat exchange occurs at the sides of the model volume. The salt body here is much smaller than the dimensions of the entire model volume, and so the boundary conditions have little influence on the thermal anomaly associated with the salt.

The boundary-value problem described above can be solved only by numerical approximation typically based on either the finite difference or the finite element method (Jensen, 1983; Corrigan and Sweat, 1995). Analytical solution is impossible, because the problem is nonlinear due to the fact that thermal conductivity varies spatially. This study uses only the finite difference method, but the inversion algorithm presented here can be implemented with either approach. For a detailed description of the finite difference method itself, readers should refer to the textbooks previously published (Ozisik, 1968; Smith, 1985).

The finite difference method subdivides the model volume in small, rectangular parallel pipes, commonly referred to as the finite difference cells. The finite difference representation of the governing equation (equation 7) is

$$\begin{aligned}&W_{i,j,k}T_{i-1,j,k}+S_{i,j,k}T_{i,j-1,k}+U_{i,j,k}T_{i,j,k-1}+P_{i,j,k}T_{i,j,k}\\&+E_{i,j,k}T_{i+1,j,k}+N_{i,j,k}T_{i,j+1,k}+D_{i,j,k}T_{i,j,k+1}=A_{i,j,k}\end{aligned} \tag{8}$$

where $W_{i,j,k}=K_{i-\frac{1}{2},j,k}\frac{\Delta y\Delta z}{\Delta x}$, $E_{i,j,k}=K_{i+\frac{1}{2},j,k}\frac{\Delta y\Delta z}{\Delta x}$, $S_{i,j,k}=K_{i,j-\frac{1}{2},k}\frac{\Delta z\Delta x}{\Delta y}$, $N_{i,j,k}=K_{i,j+\frac{1}{2},k}\frac{\Delta z\Delta x}{\Delta y}$, $U_{i,j,k}=K_{i,j,k-\frac{1}{2}}\frac{\Delta x\Delta y}{\Delta z}$, $D_{i,j,k}=K_{i,j,k+\frac{1}{2}}\frac{\Delta x\Delta y}{\Delta z}$, $A_{i,j,k}=a_{i,j,k}\Delta x\Delta y\Delta z$, and $P_{i,j,k}=-\left(K_{i+\frac{1}{2},j,k}+K_{i-\frac{1}{2},j,k}\right)\frac{\Delta y\Delta z}{\Delta x}-\left(K_{i,j+\frac{1}{2},k}+K_{i,j-\frac{1}{2},k}\right)\frac{\Delta z\Delta x}{\Delta y}-\left(K_{i,j,k+\frac{1}{2}}+K_{i,j,k-\frac{1}{2}}\right)\frac{\Delta x\Delta y}{\Delta z}$ with the downward positive Z-axis.

The finite difference equations for the entire model volume can be expressed in a simple matrix notation:

$$\mathbf{M}\boldsymbol{T}=\boldsymbol{A} \tag{9}$$

where $\mathbf{M}$ is the coefficient matrix, which is normally a band-diagonal, sparse matrix. For each row of $\mathbf{M}$, there are only seven nonzero

elements at most. $\boldsymbol{T}$ is a vector whose elements are the temperatures of all the grid cells, and $\boldsymbol{A}$ is a vector whose elements are the source terms of the all the cells.

Theoretically, the temperature values of individual grid cells can be obtained by simply multiplying $\mathbf{M}^{-1}$ to both sides of equation 9. However, attempting to do so can be computationally very expensive. The so-called direct solution of the matrix equation based on the traditional elimination scheme is slow and requires a large computational memory because it does not take advantage of the sparsity of **M**. An iterative method called biconjugate gradient method and its variants (Barret et al., 1993; Greenbaum, 1997) have become popular recently because of its robustness and speed, but they still require a considerably large memory space. After experimenting with several different approaches, the present study chose the strongly implicit procedure (SIP) (Stone, 1968; Weinstein et al., 1969) for solving equation 9. For most 3-D, steady-state diffusive problems, SIP seems to be the fastest for a given computational memory space among all the popular schemes (Hill, 1990).

Weinstein et al. (1969) gives a detailed description of the SIP computational algorithm for 3-D diffusive problems, and thus, it is not repeated here. SIP takes an iterative approach similar to the successive overrelaxation method (Press et al., 1992). For a given set of boundary conditions and thermal-conductivity distribution, the computation starts with an initial guess of the temperature distribution. Then, the temperature field is successively modified and improved to satisfy the governing equations and the boundary conditions. After several iterations, the temperature field converges. The existing iterative schemes differ in how to accelerate the convergence process. SIP typically converges with a fewer number of iterations than other methods do. Normally, the number of iterations necessary for convergence increases with the size of **M**. Another advantage of SIP is that the rate of increase is much smaller for SIP than other iterative methods. Thus, SIP is effective in solving problems with large **M**s.

REFERENCES CITED

Barret, R., M. W. Berry, T. F. Chan, J. Demmel, J. Donato, J. Dongarra, V. Eijkhout, R. Pozo, C. Romine, and H. van Vorst, 1993, Templates for the solution of Linear systems: building blocks for iterative methods: Philadelphia, Society for Industrial and Applied Mathematics, 112 p.

Beckley, L. M., and E. W. Behrens, 1993, Seismic evidence for timing of shallow salt emplacement on the Texas continental slope: Transactions— Gulf Coast Association of Geological Societies, v. 43, p. 25–30.

Blackwell, D. D., J. L. Steele, and C. A. Brott, 1980, The terrain effect on terrestrial heat flow: Journal of Geophysical Research, v. 85, p. 4757–4772.

Brigaud, F., D. S. Chapman, and S. Le Douaran, 1990, Estimating thermal conductivity in sedimentary basins using lithologic data and geophysical well logs: AAPG Bulletin, v. 74, p. 1459–1477.

Carslaw, H. S., and J. C. Jaeger, 1959, Conduction of heat in solids: Oxford, Oxford Unversity Press, 510 p.

Chunduru, R. K., M. K. Sen, P. L. Stoffa, and R. Nagendra, 1995, Non-linear inversion of resistivity profiling data for some regular geometric bodies: Geophysical Prospecting, v. 43, p. 979–1003.

Corrigan, J., and M. Sweat, 1995, Heat flow and gravity responses over salt bodies: a comparative model analysis: Geophysics, v. 60, p. 1029–1037.

Epp, D., P. J. Grim, and M. G. Langseth Jr., 1970, Heat flow in the Caribbean and Gulf of Mexico: Journal of Geophysical Research, v. 75, p. 5655–5669.

Foucher, J. P., X. Le Pichon, S. Lallemant, M. A. Hobart, P. Henry, M. Benedetti, G. K. Westbrook, and M. G. Langseth, 1990, Heat flow, tectonics, and fluid circulation at the toe of the Barbados ridge accretionary prism: Journal of Geophysical Research, v. 95, p. 8859–8867.

Greenbaum, A., 1997, Iterative methods for solving linear systems: frontiers in applied mathematics: Philadelphia, Society for Industrial and Applied Mathematics, 220 p.

Hill, M. C., 1990, Solving groundwater flow problems by conjugate-gradient methods and the strongly implicit procedure: Water Resources Research, v. 26, p. 1961–1969.

Jackson, M. P. A., and C. J. Talbot, 1989, Salt canopies: Gulf of Mexico Salt Tectonics, Gulf Coast SEPM Foundation, Tenth Annual Research Conference, p. 72–78.

Jackson, M. P. A., and C. J. Talbot, 1991, A glossary of salt tectonics: Bureau of Economic Geology, University of Texas at Austin, Austin, Texas, 44 p.

Jensen, P. K., 1983, Calculations on the thermal conditions around a salt diapir: Geophysical Prospecting, v. 31, p. 481–489.

Kirkpatrick, S., C. D. Gelatt Jr., and M. P. Vecchi, 1983, Optimization by simulated annealing: Science, v. 220, p. 671–680.

Lerche, I., and A. Lowrie, 1992, Quantitative models for the influence of salt-associated thermal anomalies on hydrocarbon generation, northern Gulf of Mexico continental margin: AAPG Bulletin, v. 76, p. 1461.

Lewis, J. F., and R. D. Hyndman, 1976, Oceanic heat flow measurements over the continental margins of eastern Canada: Canadian Journal of Earth Science, v. 13, p. 1031–1038.

Liro, L. M., 1992, Distribution of shallow salt structures, lower slope of the northern Gulf of Mexico, U.S.A.: Marine and Petrololeum Geology, v. 9, p. 433–451.

McKenna, T. E., J. Sharp Jr., and F. L. Lynch, 1996, Thermal conductivity of Wilcox and Frio sandstones in south Texas (Gulf of Mexico Basin): AAPG Bulletin, v. 80, p. 1203–1215.

Meju, M. A., 1994, Geophysical data analysis: understanding inverse problem theory and practice: Course Notes, v. 6: Tulsa, Society of Exploration Geophysicists, 296 p.

Mello, U. T., G. D. Karner, and R. N. Anderson, 1995, Role of salt in restraining the maturation of subsalt source rocks: Marine and Petroleum Geology, v. 12, p. 697–716.

Metropolis, N., A. W. Rosenbluth, M. N. Rosenbluth, and A. H. Teller, 1953, Equation of state calculations by fast computing machines: Journal of Chemical Physics, v. 21, p. 1087–1092.

Montgomery, S. L., and D. Moore, 1997, Subsalt play, Gulf of Mexico: a review: AAPG Bulletin, v. 81, p. 871–896.

Nagihara, S., and S. A. Hall, 2001, Three-dimensional gravity inversion using simulated annealing: constraints on the diapiric roots of allochthonous salt structures: Geophysics, v. 66, p. 1438–1449.

Nagihara, S., J. G. Sclater, L. M. Beckley, E. W. Behrens, and L. A. Lawver, 1992, High heat flow anomalies over salt structures on the Texas continental slope, Gulf of Mexico: Geophysical Research Letters, v. 19, p. 1687–1690.

Nagihara, S., L. M. Beckley, E. W. Behrens, and J. G. Sclater, 1993, Characteristics of heat flow through diapiric salt structures on the Texas continental slope: Transactions— Gulf Coast Association of Geological Societies, v. 43, p. 269–279.

Nagihara, S., J. G. Sclater, J. D. Phillips, E. W. Behrens, T. Lewis, L. A. Lawver, Y. Nakamura, J. Garcia-Abdeslem, and A. E. Maxwell, 1996, Heat flow in the western abyssal plain of the Gulf of Mexico: implications for thermal evolution of the old oceanic lithosphere: Journal of Geophysical Research, v. 101, p. 2895–2913.

O'Brien, J. J., and I. Lerche, 1984, The influence of salt domes on

paleotemperature distributions: Geophysics, v. 49, p. 2032–2043.
O'Brien, J. J., and I. Lerche, 1988, Impact of heat flux anomalies around salt diapirs and salt sheets in the Gulf Coast on hydrocarbon maturity: models and observations: Transactions— Gulf Coast Association of Geological Societies, v. 38, p. 231–243.
Ozisik, M. N., 1968, Boundary value problems of heat conduction: New York, Dover Publications, 504 p.
Press, W. H., S. A. Teukolsky, W. T. Vetterling, and B. P. Flannery, 1992, Numerical recipes in Fortran 77: Cambridge, Cambridge University Press, 933 p.
Press, W. H., S. A. Teukolsky, W. T. Vetterling, and B. P. Flannery, 1996, Numerical Recipes in Fortran 90— the art of parallel scientific computing: Cambridge, Cambridge University Press, 1486 p.
Ratcliff, D. W., and D. J. Weber, 1997, Geophysical imaging of subsalt geology: The Leading Edge, v. 16, p. 115–142.
Ratcliff, D. W., S. H. Gray, and N. D. Whitmore Jr., 1992, Seismic imaging of salt structures in the Gulf of Mexico: Geophysics: Leading Edge of Exploration, v. 11, p. 15–31.
Salvador, A., 1987, Late Triassic–Jurassic paleogeography and origin of Gulf of Mexico Basin: AAPG Bulletin, v. 71, p. 419–451.
Salvador, A., 1991, Origin and development of the Gulf of Mexico Basin, *in* A. Salvador, ed., The Gulf of Mexico Basin: the geology of North America: Boulder, Geological Society of America, p. 389–444.
Sawyer, D. S., R. T. Buffler, and R. H. Pilger Jr., 1991, The crust under the Gulf of Mexico basin, *in* A. Salvador, ed., The Gulf of Mexico Basin: geology of North America: Boulder, Geological Society of America, p. 53–72.
Selig, F., and G. C. Wallick, 1966, Temperature distribution in salt domes and surrounding sediments: Geophysics, v. 49, p. 2032–2043.
Sen, M., and P. L. Stoffa, 1995, Global optimization methods in geophysical inversion: advances in exploration geophysics, v. 4: Amsterdam, Elsevier, 281 p.
Sen, M., and P. L. Stoffa, 1996, Baysian inference, Gibbs' sampler and uncertainty estimation in geophysical inversion: Geophysical Prospecting, v. 44, p. 313–350.
Seni, S. J., 1992, Evolution of salt structures during burial of salt sheets on the slope, northern Gulf of Mexico: Marine and Petroleum Geology, v. 9, p. 452–468.
Seni, S. J., and M. P. A. Jackson, 1992, Segmentation of salt allochthons: Geology, v. 20, p. 169–172.
Smith, G. D., 1985, Numerical solution of partial differential equations: finite difference methods: London, Oxford University Press, 337 p.
Stone, H., 1968, Iterative solution of implicit approximations of multidimensional partial differential equations: Society for Industrial and Applied Mathematics Journal on Numerical Analysis, v. 5, p. 530–558.
Tari, G. C., P. R. Ashton, K. L. Coterill, J. S. Molnar, M. C. Sorgenfrei, W. A. Philip-Thompson, D. W. Valasek, and J. F. Fox, 2002, Are west Africa deepwater salt tectonics analogous to the Gulf of Mexico?: Oil & Gas Journal, v. 100.9 (March 4), p. 73–81.
Vizgirda, J., J. J. O'Brien, and I. Lerche, 1985, Thermal anomalies on the flanks of a salt dome: Geothermics, v. 14, p. 553–565.
Von Herzen, R. P., H. Hoskins, and T. H. Van Andel, 1972, Geophysical studies in the Angola diapir field: Geological Society of America Bulletin, v. 83, p. 1901–1910.
Watkins, J. S., W. R. Bryant, and R. T. Buffler, 1996, Structural framework map of the northern Gulf of Mexico, *in* J. O. Jones and R. L. Freed, eds., Structural framework of the northern Gulf of Mexico: Austin, Texas, Gulf Coast Association of Geological Societies, p. 95–98.
Weinstein, H. G., H. L. Stone, and T. V. Kwan, 1969, Iterative procedure for solution of systems of parabolic and elliptic equations in three dimensions: Industrial Engineering and Chemistry Fundamentals, v. 8, p. 281–287.
Worrall, D. M., and S. Snelson, 1989, Evolution of the northern Gulf of Mexico, with emphasis on Cenozoic growth faulting and the roles of salt, *in* A. W. Bally and A. R. Palmer, eds., The geology of North America—an overview: Geological Society of America, Decade of North American Geology, v. A, p. 97–138.
Yang, J. M., 1981, Thermophysical properties, *in* L. H. Gevantman, ed., Physical properties data for rock salt: National Bureau of Standards Monograph: Washington, U.S. Government Printing Office, p. 205–221.